

Palladium K-edge X-ray Absorption Spectroscopy Studies on Controlled Ligand Systems

Luke P. Westawker, Julia K. Khusnutdinova, Rachel F. Wallick, and Liviu M. Mirica*

Cite This: *Inorg. Chem.* 2023, 62, 21128–21137

Read Online

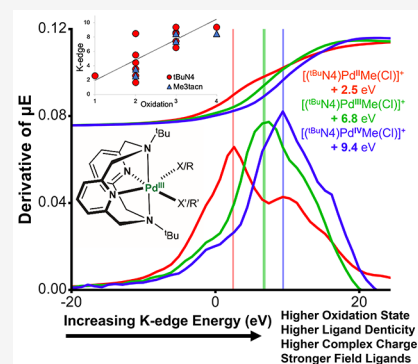
ACCESS |

Metrics & More

Article Recommendations

Supporting Information

ABSTRACT: X-ray absorption spectroscopy (XAS) is widely used across the life and physical sciences to identify the electronic properties and structure surrounding a specific element. XAS is less often used for the characterization of organometallic compounds, especially for sensitive and highly reactive species. In this study, we used solid- and solution-phase XAS to compare a series of 25 palladium complexes in controlled ligand environments. The compounds include palladium centers in the formal I, II, III, and IV oxidation states, supported by tridentate and tetradentate macrocyclic ligands, with different halide and methyl ligand combinations. The Pd K-edge energies increased not only upon oxidizing the metal center but also upon increasing the denticity of the ligand framework, substituting sigma-donating methyl groups with chlorides, and increasing the charge of the overall metal complex by replacing charged ligands with neutral ligands. These trends were then applied to characterize compounds whose oxidation states were otherwise unconfirmed.



INTRODUCTION

X-ray absorption spectroscopy (XAS) is used across heterogeneous catalysis, geology, biology, material science, and physics to identify the environment surrounding a specific element.^{1–8} XAS is less often used to characterize organometallic compounds and homogeneous catalysts, especially under reactive *in situ* conditions.^{9–14} The hard X-rays required for such K-edge studies allow samples to be in the solid or solution phase, as well as in very dilute samples.¹⁵ The X-ray absorption near edge structure (XANES) region, which involves dipole-allowed transitions from the 1s orbital to the unoccupied p-orbitals, carries information about the local geometry surrounding the metal center.^{16,17} This study shows how further analysis of the K-edge XANES region of metal complexes supported by a controlled ligand system can unambiguously determine the oxidation state, solution phase coordination geometry, and ligand substitution for a series of systematically modified complexes.

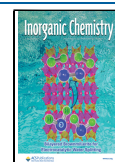
Metal centers involved in heterogeneous catalysis such as vanadium, titanium, and iron have been extensively studied by XAS and have recently been the focus of intensive computational modeling to further interpret pre-edge features to assign second sphere coordination interactions, leading the way to 3D structural determination of compounds and increased mechanistic insight.^{18–21} A similar approach can be taken with palladium complexes, which are relatively underexplored using XANES, to fully understand the solution-phase properties of catalytically relevant organometallic compounds.^{22,23}

Palladium is a versatile transition metal that can access various oxidation states (0, I, II, III, and IV),^{24–32} enabling efficient catalysis for C–C coupling, C–H functionalization,

and hydrocarbon oxidation reactions.^{32–35} It has recently been shown that high-valent Pd(III) and Pd(IV) species are active intermediates in several stoichiometric and catalytic C–C and C–heteroatom bond transformations, followed by reductive elimination of a C–X bond.^{24,25,27,28,30–32,36–43} Although Pd(0), Pd(II), and Pd(IV) complexes are ubiquitous in catalysis, much less is known about Pd(I) and Pd(III) systems, which are often implicated as reactive intermediates but are EPR-silent in their common binuclear form. We previously isolated the first organometallic mononuclear Pd(I) complexes using a ^tBu₄N₄ ligand³² and isolated the first binuclear Pd(III) complexes that are not stabilized by a Pd–Pd bond by using a tridentate nitrogen-donor ligand *N,N',N''*-trimethyl-1,4,7-triazacyclononane (Me₃tacn).^{32,44} Given our interest in Pd(III) chemistry,^{36,45–52} probing the ligand effects on these Pd(III) complexes can provide insights into organometallic reactivity and future catalytic design.

Palladium K-edge XAS, which involves excitation of a 1s core electron to the unoccupied 5p orbitals, has been shown to be a qualitative way to further probe the electronic environment of a Pd center.^{53–55} One of the few studies into organometallic Pd XAS saw an increase of 1 eV in the K-edge energy per increase in oxidation state for several

Received: August 30, 2023
Revised: October 24, 2023
Accepted: October 26, 2023
Published: December 1, 2023



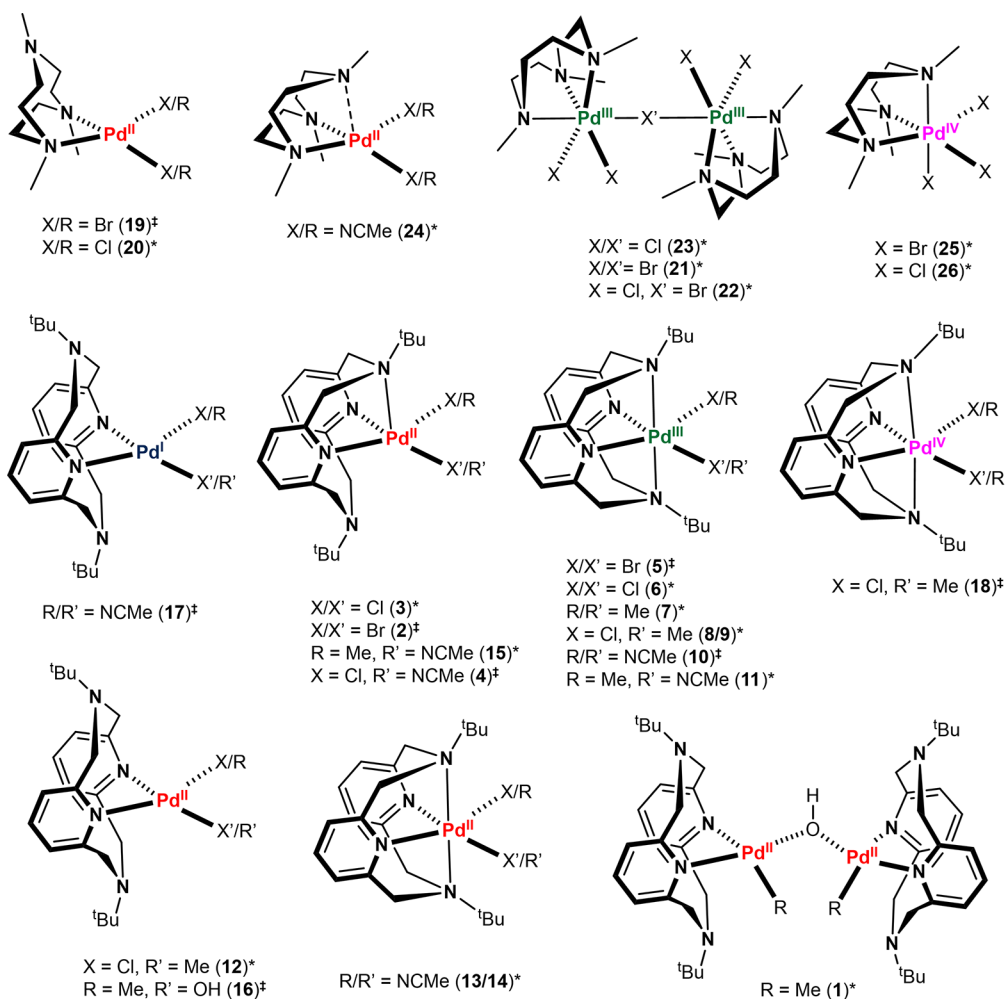


Figure 1. Structures of compounds 1–26 based on crystal structures (*) or proposed coordination (‡) consistent with experimental data and analogous compounds. Overall molecular charges and counterions are not depicted.

complexes, which was subsequently used to monitor the redox chemistry *in situ*.^{53–55} Another study showed some dependence of edge energy on the bidentate phosphine ligand backbone.⁵⁶ In our cases, we observe similar trends upon redox changes and ligand substitution reactions but the magnitude of change in edge energy varies across systems.

In this study, we compare an array of 25 Pd complexes in comparable ligand environments, whose K-edge energies shift upon changes in the oxidation state or ligand environment (Figure 1 and Table 1). The compounds include palladium centers in the formal I, II, III, and IV oxidation states, supported by bidentate, tridentate, and tetradentate macrocyclic ligands with different halide and methyl ligand combinations. Based on the analysis of the K-edge energies, it was observed that these energies increase not only upon oxidation of the metal center but also upon increasing denticity of the ligand framework, lowering the strength of the ligand field, and increasing the charge of the overall metal complex by replacing charged ligands with neutral ligands. These trends were then applied to characterize compounds whose oxidation states were otherwise unconfirmed.

We previously used XAS to aid in the characterization of a Pd(I) compound.⁵⁷ Since then, we have been able to perform a systematic study to assist in further oxidation state confirmation as well as observe trends across different ligands.

We have shown that XAS can be used to study organometallic redox chemistry for a system in a similar or consistent ligand environment. As opposed to the Pd pre-edge features, which are often used for comparing oxidation states within a series of complexes of identical coordination environments,⁵⁵ the energy of the Pd rising K-edge is less sensitive to a metal's coordination number, allowing for comparison between the flexible Me₃tacn and ^tBuN₄ ligand frameworks (Figure 1). We also provide insight into comparisons between ligand systems, expanding on the previous literature that compared K-edge data for Pd(0) and Pd(II) redox for a single ligand system⁵⁵ to a wider range of Pd(I), Pd(II), Pd(III), and Pd(IV) complexes with different ligands.

EXPERIMENTAL DETAILS

General Procedure. All experiments and manipulations were performed under a nitrogen atmosphere using standard Schlenk and glovebox techniques, if not indicated otherwise. All reagents for which synthesis is not given were commercially available from Sigma-Aldrich, Acros Organics, Strem Chemicals, or Pressure Chemical and were used as received without further purification. Solvents were purified prior to use by passing through a column of activated alumina using an MBraun, Inc. SPS.

Preparation. We have previously reported the syntheses for compounds 19–26,⁴⁶ compounds 7 and 8/9,⁴⁵ compounds 6, 11, and 13/14,³⁶ and compounds 10 and 17.⁶² Compound 18¹⁷ and

Table 1. K-Edge Energy Levels of Compounds 1–26 Relative to the Pd Foil (27)^a

#	K-edge (eV)	Name	Nuclearity	Pd OS	Framework	R/X	R'/X'	Phase	X-ray	Charge	Pd CN	Ref.
1	2.4 ± 0.1	[(^t Bu ₄ NPd ^{II} Me) ₂ OH] ⁺	binuclear	2	^t Bu ₄ N4	Me	OH	solid	yes ⁴⁷	+1	4	47
2	3.6 ± 0.2	^t Bu ₄ N4Pd ^{II} Br ₂	mononuclear	2	^t Bu ₄ N4	Br	Br	solid	none	0	5 [‡]	58
3	3.7 ± 0.2	^t Bu ₄ N4Pd ^{II} Cl ₂	mononuclear	2	^t Bu ₄ N4	Cl	Cl	solid	yes ³⁶	0	5	59–60
4	5.2 ± 0.2	[^t Bu ₄ N4Pd ^{II} Cl(MeCN)] ⁺	mononuclear	2	^t Bu ₄ N4	Cl	MeCN	solid	none	+1	5 [‡]	this work
5	7.5 ± 0.2	[^t Bu ₄ N4Pd ^{III} Br ₂] ⁺	mononuclear	3	^t Bu ₄ N4	Br	Br	solid	this	+1	6	this work
6	7.8 ± 0.1	[^t Bu ₄ N4Pd ^{III} Cl ₂] ⁺	mononuclear	3	^t Bu ₄ N4	Cl	Cl	solid	yes ³⁶	+1	6	36, 60
7	6.2 ± 0.2	[^t Bu ₄ N4Pd ^{III} Me ₂] ⁺	mononuclear	3	^t Bu ₄ N4	Me	Me	solid	yes ⁴⁷	+1	6	36, 45, 47
8	7.2 ± 0.2	[^t Bu ₄ N4Pd ^{III} Me(Cl)] ⁺	mononuclear	3	^t Bu ₄ N4	Cl	Me	solid	yes ⁴⁵	+1	6	17, 36, 45, 60–61
9	6.8 ± 0.2	[^t Bu ₄ N4Pd ^{III} Me(Cl)] ⁺	mononuclear	3	^t Bu ₄ N4	Cl	Me	solution	yes ⁴⁵	+1	6	17, 36, 45, 60–61
10	10.5 ± 0.4	[^t Bu ₄ N4Pd ^{III} (MeCN) ₂] ³⁺	mononuclear	3	^t Bu ₄ N4	MeCN	MeCN	solution	none	+3	6 [‡]	62
11	8.7 ± 0.4	[^t Bu ₄ N4Pd ^{III} Me(MeCN) ₂] ²⁺	mononuclear	3	^t Bu ₄ N4	Me	MeCN	solution	yes ³⁶	+2	6	36
12	2.5 ± 0.1	^t Bu ₄ N4Pd ^{II} Me(Cl)	mononuclear	2	^t Bu ₄ N4	Cl	Me	solid	yes ³⁶	0	4	17, 36, 45, 59–60
13	7.0 ± 0.5	[^t Bu ₄ N4Pd ^{II} (MeCN) ₂] ²⁺	mononuclear	2	^t Bu ₄ N4	MeCN	MeCN	solid	yes ³⁶	+2	6	36, 57
14	7.0 ± 0.6	[^t Bu ₄ N4Pd ^{II} (MeCN) ₂] ²⁺	mononuclear	2	^t Bu ₄ N4	MeCN	MeCN	solution	yes ³⁶	+2	6	36, 57
15	2.3 ± 0.2	[^t Bu ₄ N4Pd ^{II} Me(MeCN)] ⁺	mononuclear	2	^t Bu ₄ N4	Me	MeCN	solid	none	+1	5 [‡]	36, 59
16	3.0 ± 0.2	^t Bu ₄ N4Pd ^{II} Me(OH)	mononuclear	2	^t Bu ₄ N4	Me	OH	solution	none	0	4 [‡]	47
17	1.9 ± 0.1	[^t Bu ₄ N4Pd ^{II} (MeCN) ₂] ⁺	mononuclear	1	^t Bu ₄ N4	MeCN	MeCN	solution	none	+1	4 [‡]	57
18	9.4 ± 0.1	[^t Bu ₄ N4Pd ^{IV} MeCl] ₂ ²⁺	mononuclear	4	^t Bu ₄ N4	Cl	Me	solution	none	+2	6 [‡]	17
19	3.1 ± 0.1	Me ₃ tacnPd ^{II} Br ₂	mononuclear	2	Me ₃ tacn	Br	Br	solid	none	0	4 [‡]	63
20	3.6 ± 0.2	Me ₃ tacnPd ^{II} Cl ₂	mononuclear	2	Me ₃ tacn	Cl	Cl	solid	yes ⁴⁶	0	4	63
21	8.3 ± 0.2	[(Me ₃ tacnPd ^{III}) ₂ Br ₅] ⁺	binuclear	3	Me ₃ tacn	Br	Br	solid	yes ⁴⁶	+1	6	32, 63
22	8.2 ± 0.1	[(Me ₃ tacnPd ^{III}) ₂ Cl ₄ Br] ⁺	binuclear	3	Me ₃ tacn	Cl	Br	solid	yes ⁴⁶	+1	6	63–64
23	8.3 ± 0.1	[(Me ₃ tacnPd ^{III}) ₂ Cl ₅] ⁺	binuclear	3	Me ₃ tacn	Cl	Cl	solid	yes ⁴⁶	+1	6	63–64
24	4.6 ± 0.4	[Me ₃ tacnPd ^{II} (MeCN) ₂] ²⁺	mononuclear	2	Me ₃ tacn	MeCN	MeCN	solid	yes ⁶⁵	+2	5	63, 65
25	9.2 ± 0.3	[Me ₃ tacnPd ^{IV} Br ₃] ⁺	mononuclear	4	Me ₃ tacn	Br	Br	solution	yes ⁴⁶	+1	6	63
26	9.4 ± 0.1	[Me ₃ tacnPd ^{IV} Cl ₃] ⁺	mononuclear	4	Me ₃ tacn	Cl	Cl	solution	yes ⁴⁶	+1	6	63
27	0.1 ± 0.1	Pd foil (reference)	mononuclear	0								

^aOxidation states are indicated with Pd(I) as blue, Pd(II) as red, Pd(III) as green, and Pd(IV) as pink. The ligand frameworks are ^tBu₄N4 (blue), Me₃tacn (orange). Additional ligands include halide (green), methyl (orange), acetonitrile (blue), and hydroxide (yellow). Published syntheses are referenced. Coordination numbers are from crystal structures or predicted ([‡]).

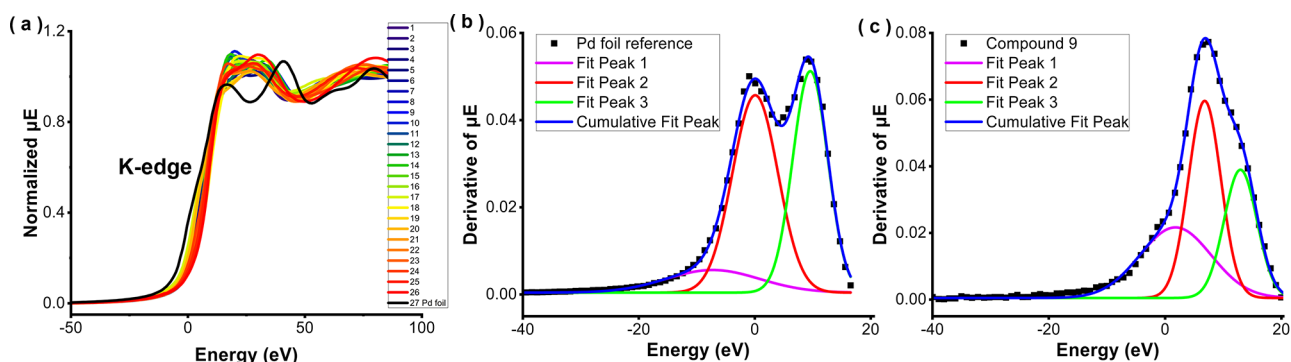


Figure 2. (a) Normalized absorption spectra of compounds 1–26 reported in eV with respect to the K-edge of the Pd foil (black line). The K-edge of our compounds range from +1 to +10 eV greater than that of the Pd foil. The peak fitting of the first derivative of the XANES K-edge is shown for (b) the reference Pd foil and (c) compound 9 to three Gaussian functions. The peak energy is determined by the center, most intense peak to give values of 0.08 ± 0.08 for the Pd foil and 6.50 ± 0.20 for compound 9, with R^2 values of 0.998 and 0.997, respectively.

compounds 3, 12, and 15⁵⁹ were synthesized by following previously reported procedures. The characterization for compounds 2, 4, and 5 is provided in the [Supporting Information](#), Section VII.

X-ray Structure Determination. Crystal structures have been reported for compounds 1 and 7,⁴⁷ compounds 3, 6, and 11–14,³⁶ compounds 20–26,⁶³ and compound 8/9.⁴⁵ The previously unreported crystal structure for compound 5 is provided in the [Supporting Information](#), Section VIII.

X-ray Absorption Spectroscopy (XAS) Studies. Pd K-edge XANES measurements were performed at beamline 10-ID of the advanced photon source (APS).^{66,67} Solid-phase samples were measured in transmission mode, and solution-phase samples were measured in partial fluorescence yield using a 13-element Ge detector. The energy was calibrated with a Pd(0) foil measured in tandem with the samples ([Figure 2](#) and [Table S1](#)). The samples were loaded into a custom-designed, chemically resistant PEEK cell fitted with a cap with a Swagelok VCR fitting and a hand-tightened O-ring

seal.^{17,57} Many of these complexes are thermally unstable at room temperature and nonisolable; thus, some measurements were performed in -10 °C acetonitrile solutions ([Table 1](#)). In addition, temperature- and air-sensitive samples were loaded under a nitrogen blanket in a dry ice bath. Samples 9/14/16 were measured in the solution-phase in room temperature acetonitrile at a concentration of 5 mM. Samples 10/11/17/18/25/26 were measured in the solution phase at -10 °C in acetonitrile also at a concentration of 5 mM. All other samples were measured in the solid phase at room temperature, with 3 mg of compound per sample. All spectra are the result of merging two-six scans of a sample immediately following acquisition.

XAS Spectral Processing and Analysis. The program Athena⁶⁸ was used to perform background subtraction and normalization of the XANES spectra. The Pd foil reference for every sample was energy corrected by selecting the maximum in the first derivative, finding the zero crossing in the second derivative, and setting the energy of the zero crossing to 24350 eV.⁶⁹ The energy-corrected Pd foil reference

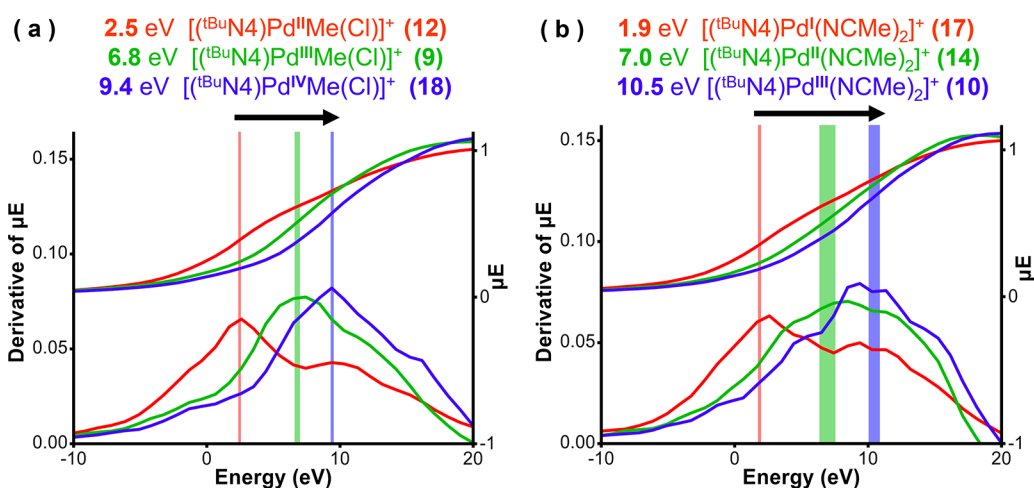


Figure 3. Comparison of relative XANES K-edge energies for the (a) $(t\text{Bu}_4\text{N}_4)\text{PdMe}(\text{Cl})$ system with varying oxidation states: Pd(II) is red (12), Pd(III) is green (9), and Pd(IV) is blue (18), and for the (b) $(t\text{Bu}_4\text{N}_4)\text{Pd}(\text{NCMe})_2$ system with varying oxidation states: Pd(I) is red (17), Pd(II) is green (14), and Pd(III) is blue (10).⁵⁷ The top lines show the XANES normalized energy curves corresponding to the rightmost y-axes, while the bottom lines show their derivatives corresponding to the leftmost y-axes. The K-edge energy is measured as the first derivative's maximum peak, depicted by the vertical lines, where the error is denoted by the width of the line, displaying the statistical significance between values. Energies are reported relative to the K-edge of the Pd foil. Solid-phase 8 and 13 are analogous with their solution-phase versions 9 and 14, respectively.

Table 2. Oxidation State Trends for Compounds with Identical Bound Ligands, Showing the Consistent Trend of Increasing K-Edge XANES Energy as Pd(I) < Pd(II) < Pd(III) < Pd(IV) with Energies Reported in eV Relative to the K-edge of Pd Foil

Compounds	Framework	X/R	X'/R'	Oxidation State			
				Pd(I)	Pd(II)	Pd(III)	Pd(IV)
19/21/25	Me ₃ tacn	Br	Br		3.1 ± 0.1	8.3 ± 0.2	9.1 ± 0.1
20/23/26	Me ₃ tacn	Cl	Cl		3.6 ± 0.2	8.3 ± 0.1	9.4 ± 0.1
2/5	$t\text{Bu}_4\text{N}_4$	Br	Br		3.6 ± 0.2	7.5 ± 0.2	
3/6	$t\text{Bu}_4\text{N}_4$	Cl	Cl		3.7 ± 0.2	7.8 ± 0.1	
12/08/18	$t\text{Bu}_4\text{N}_4$	Me	Cl		2.5 ± 0.1	7.2 ± 0.2	9.4 ± 0.1
15/11	$t\text{Bu}_4\text{N}_4$	Me	MeCN		2.3 ± 0.2	8.7 ± 0.4	
17/13/10	$t\text{Bu}_4\text{N}_4$	MeCN	MeCN	1.9 ± 0.1	7.0 ± 0.5	10.5 ± 0.4	

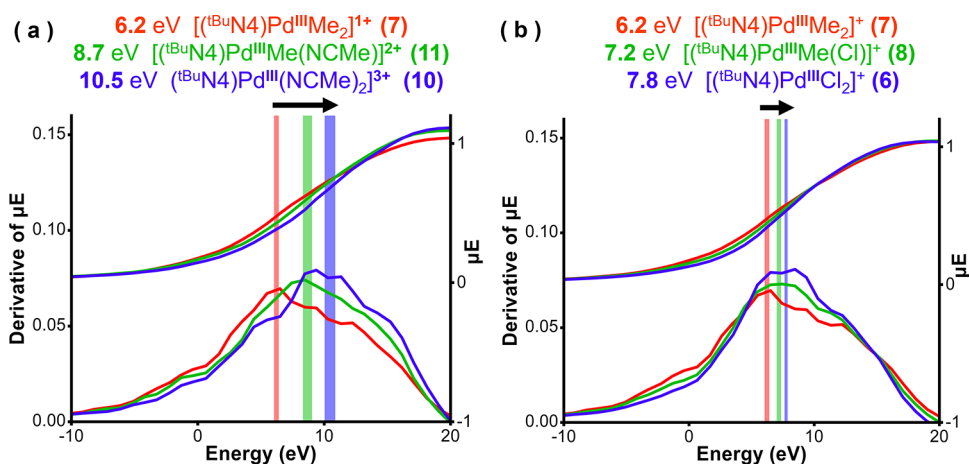


Figure 4. Series of $t\text{Bu}_4\text{N}_4\text{Pd}^{\text{III}}$ compounds where (a) charged methyl groups are progressively replaced by neutral acetonitrile ligands for compounds 7, 10, and 11, and where (b) strong sigma donor methyl groups are replaced with chloride for compounds 6, 7, and 8/9. Energies are reported relative to the K-edge of Pd foil. The top lines show the XANES normalized energy curves corresponding to the rightmost y-axes, while the bottom lines show their derivatives corresponding to the leftmost y-axes. Vertical lines indicate the K-edge energy and errors of the fit on either side.

spectra were then aligned so that all data were on the same absolute energy grid for analysis. The energy of the K-edge was determined by taking the first derivative of the normalized spectra of the K-edge and fitting it to three gaussians (Figure 2 and Table S1), consistent with excitation of a 1s electron into three unfilled 5p orbitals. All fits had R^2 values greater than 0.99, as shown in the Supporting Information,

Section II. The peak energy of each compound is defined as the white line, observed in Figure 2b as the middle red peak 2. The error of this peak was always less than 0.6 eV (Table 1). The K-edge energies of all compounds were calibrated to the Pd foil edge energy of 24350 eV, which is defined as 0 eV herein.

RESULTS AND DISCUSSION

Effect of Oxidation State. For similar ligand environments, a higher metal oxidation state has a higher K-edge energy across the complete series of Pd(I) < Pd(II) < Pd(III) < Pd(IV) compounds. The first oxidation caused the greatest increase in K-edge energy compared to consecutive oxidations, showing a nonlinear correspondence between the edge energy and the oxidation state (Figure 3, Table 2). Further comparison is shown in the Supporting Information, Section III.

Effect of Electron Donating Ligands. When the formal charge and oxidation states were kept constant for Pd(III), the K-edge energy decreased upon replacement of halide (Cl⁻) groups with strongly sigma-donating methyl groups (CH₃⁻), as seen in Figure 4 and Tables 3 and 4. This is consistent with methyl groups adding electron density to the metal center, paralleling the observed decrease in K-edge energy with decreasing oxidation state.

Table 3. Effect of X/R Groups on Pd XANES K-Edge Energy Reported in eV for ^tBu₄N₄Pd^{III}RX Compounds 6, 7, 8/9, 10, and 11^a

[(^t Bu ₄ N ₄)Pd ^{III} RX] ⁺	X/R	-Cl	-Me	-NCMe	
6/8	-Cl	7.8 ± 0.1	7.2 ± 0.2		Weak Field
8/7/11	-Me	7.2 ± 0.2	6.2 ± 0.2	8.7 ± 0.4	Strong Field
					Charged Ligand
11/10	-NCMe		8.7 ± 0.4	10.5 ± 0.4	Neutral Ligand

^aArrows show an increase in edge energy due to weaker field ligands (blue) or increase in complex charge (orange). Compound 5, [^tBu₄N₄Pd^{III}Br₂]⁺, also fits this trend. Energies are reported relative to the K-edge of Pd foil.

Table 4. Effect of X/R Groups on Pd XANES K-Edge Energy for ^tBu₄N₄Pd^{II}RX Compounds 3, 4, 12, 13/14, 15, and 16^a

(^t Bu ₄ N ₄)Pd ^{II} RX	X/R	-Cl	-NCMe	-OH	
3/4	-Cl	3.7 ± 0.2	5.2 ± 0.2		Weak Field
12/15/16	-Me	2.5 ± 0.1	2.3 ± 0.2	3.0 ± 0.2	Strong Field
					Charged Ligand
4/13	-NCMe	5.2 ± 0.2	7.0 ± 0.5		Neutral Ligand

^aArrows show an increase in edge energy due to weaker field ligands (blue) or an increase in complex charge (orange). Compound 2, ^tBu₄N₄Pd^{II}Br₂, also fits this trend. Energies are reported in eV relative to the K-edge of Pd foil.

Effect of Molecular Charge. When the oxidation states were kept constant, charged methyl groups (CH₃⁻) were replaced with neutral acetonitrile ligands (MeCN), increasing the overall charge for the Pd(III) complexes 7/11/10 (Table 3) and for Pd(II) complexes 4/12/13/15 (Table 2), often requiring more cations. Complexes with a higher overall charge due to neutral ligands exhibited higher K-edge energies, paralleling the observed increase in K-edge energy with an increasing Pd oxidation number (Tables 3 and 4). Further comparisons are shown in the Supporting Information, Section V.

Competing Effects. When complex charge and ligand field strength are increased simultaneously, such as exchanging

Cl⁻ with MeCN, the K-edge energies increase going from [^tBu₄N₄Pd^{II}Cl₂]⁰ (3) to [^tBu₄N₄Pd^{II}(MeCN)Cl]¹⁺ (4) to [^tBu₄N₄Pd^{II}(MeCN)₂]²⁺ (13/14). This correlates with an increased complex charge as well as going from a 5-coordinate to 6-coordinate metal center (Figure 1) but is inconsistent with the increase in the ligand field strength. This is also the case when compound 8/9 is changed to 11. Similarly, the XANES spectra of the charged 5-coordinate species [^tBu₄N₄Pd^{II}Me(MeCN)]⁺ (15) is blue-shifted compared to the neutral 4-coordinate species [^tBu₄N₄Pd^{II}Me(Cl)]⁰ (12). For all these systems, the overall complex charge has a greater effect on the K-edge energy than the changes in ligand field strength (Figure 4), as further shown in the Supporting Information, Sections III–V.

Effect of Ligand Framework. Comparing the two ligand frameworks revealed that ^tBu₄N₄ compounds exhibited a slightly higher energy K-edge values than analogous Me₃tacn compounds (Figure 5a,b), specifically for compounds 2 versus 19 and 13/14 versus 24. This is consistent with ^tBu₄N₄ being a tetradentate ligand that can donate more electron density to the Pd atom than tridentate Me₃tacn. However, this distinction in K-edge energy can often be statistically insignificant, as seen for compounds 20/3. When other factors become involved, such as Me₃tacn forming binuclear compounds 21/23 with five halides compared to the ^tBu₄N₄ mononuclear compounds 5/6 with two halides, the Me₃tacn species show a large K-edge value, potentially due to the increased amount of electron density around the Pd center in the dinuclear species.

The ability of ^tBu₄N₄ to change denticity also appears to correspond with the K-edge changes due to the ligand strength and complex charges. For instance, when replacing a stronger field methyl ligand with a weak field halide ligand, [^tBu₄N₄Pd^{II}Me(Cl)]⁰ (12) increased in energy to [^tBu₄N₄Pd^{II}Cl₂]⁰ (3), corresponding with coordination number increasing as the ^tBu₄N₄ binding mode changes from bidentate to tridentate (Figure 1 and Table 4). While there is no crystal structure for 4, its relatively high K-edge value suggests a coordination number greater than those of compounds 15 and 12.

Insight into 5p Orbitals. For the Me₃tacn compounds that are octahedral around the Pd center (Figure 1), the fitted third Gaussian peak was determined to be an almost insignificant horizontal line as seen for compounds 21/22/23/25/26 (Figure 5f). These compounds appear to have only one primary peak, so 2-Gaussian fitting obtained R² values greater than 0.99 and with low fit errors, as shown in the Supporting Information, Section II. However, the square planar (Me₃tacn)Pd compounds (19/20) have an additional peak and need a 3-Gaussian fitting. All ^tBu₄N₄ (1–18) complexes required a 3-Gaussian fit and have three distinct peaks.

Since the K-edge corresponds to the excitation of 1s electrons into three empty 5p orbitals, the presence of multiple peaks in the first derivative suggests that the 5p orbitals are not degenerate. The crystal structures depicted in Figure 1 show that the octahedral complexes (21/22/23/25/26) with a tridentate Me₃tacn have potential 3-fold symmetry that would correlate with degeneracy in p-orbitals. Part of this degeneracy would be lost when going to a square planar geometry (19/20) with a bidentate Me₃tacn, corresponding with the observed splitting of peaks, which is also observed with the pseudotridentate (24) framework. Conversely, ^tBu₄N₄ com-

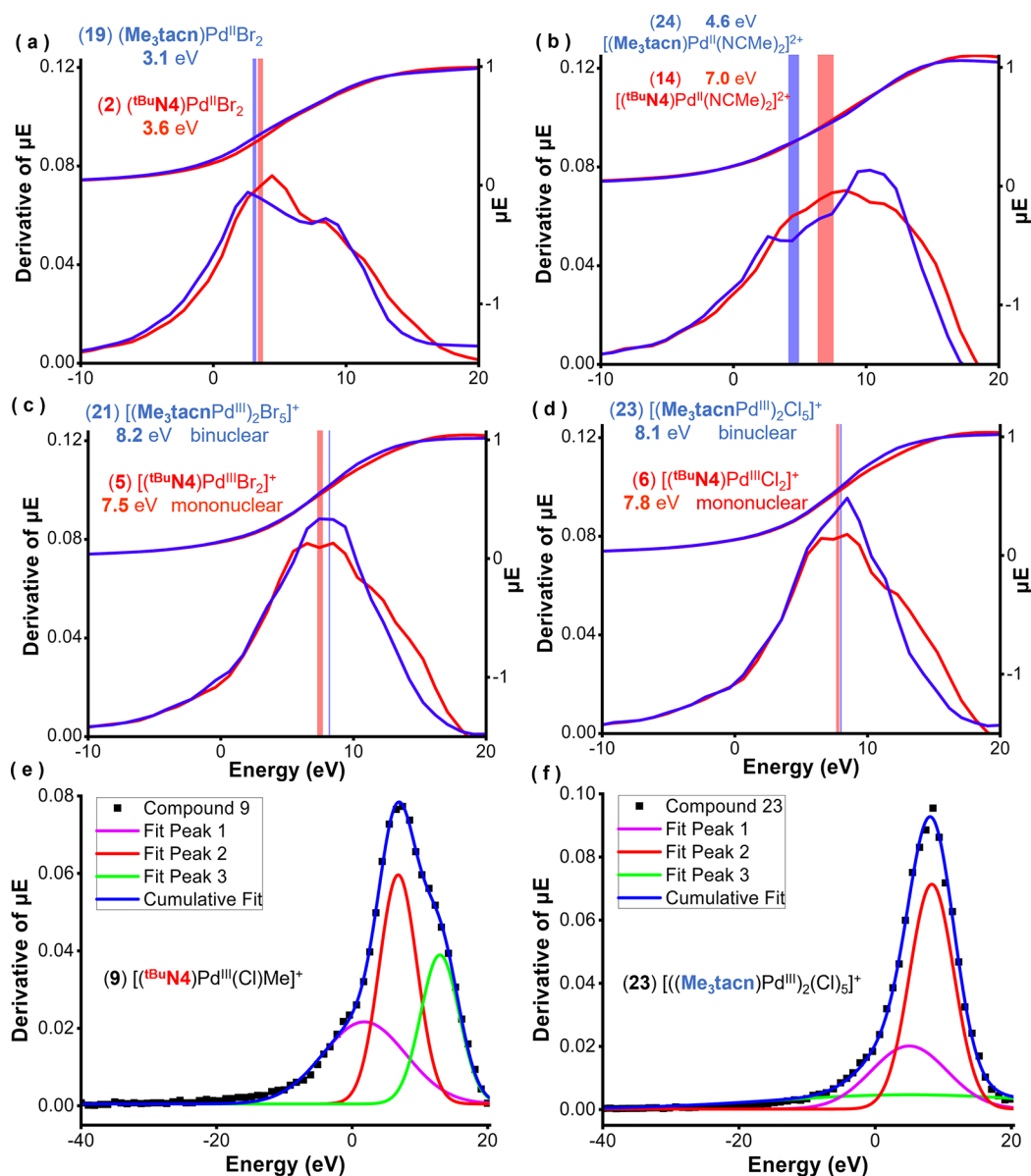


Figure 5. Effect of ligand frameworks on (a) $\text{Pd}^{\text{II}}\text{Br}_2$ for compounds 2 and 19, (b) $\text{Pd}^{\text{II}}(\text{MeCN})_2$ for compounds 13/14 and 24, (c) $\text{Pd}^{\text{III}}(\text{Br})_x$ for compounds 5 and 21, and (d) $\text{Pd}^{\text{III}}\text{Cl}_x$ for compounds 6 and 23. The tBu_4N compounds are shown in red, and the Me_3tacn compounds are shown in blue. Vertical lines indicate the K-edge energy and the errors of the fit on either side. Additionally, comparisons between the 3-Gaussian fits are shown for (e) the tetradentate $[\text{tBu}_4\text{N}4\text{Pd}^{\text{III}}\text{Me}(\text{Cl})]^+$ compound 9 with low p-orbital symmetry, and (f) the tridentate $[(\text{Me}_3\text{tacn})_2\text{Pd}^{\text{III}}]_2(\text{Cl})_5^+$ compound 23 with high p-orbital symmetry.

pounds always have 2–3 peaks as the ligand cannot have more than 2-fold symmetry and is often further distorted. Fitting the Pd K-edge to Gaussian peaks may give further insight into the coordinate environment and denticity of flexible ligand frameworks.

Solid vs Solution Phase. The edge energies of analogous solid and solution samples were not statistically distinct, suggesting that they retained the same coordination environment (Figure 6) and that the presence of solvent does not significantly affect the $1s \rightarrow 5p$ energy transition of the Pd center. However, since these ligand frameworks have flexible arms, it is possible that larger deviations in spectra might suggest variations in the coordination number.

Confirmation of Previously Ambiguous Oxidation States. The consistent trend of increasing K-edge energies for higher oxidation states for a comparable ligand environment

was then applied to confirm the identity of EPR-silent compounds whose oxidation states were still unconfirmed such as mononuclear Pd(II) and binuclear Pd(III) compounds. This was important for studying the $(\text{Me}_3\text{tacn})\text{Pd}$ dihalide series of compounds 19–23 and 25–26, where a mononuclear Pd(II) species is oxidized to an EPR-silent binuclear Pd(III) complex, followed by an oxidation to mononuclear Pd(IV) species. In these cases, the K-edge energies for the Pd(III) complexes fall between the energies for the Pd(II) and Pd(IV) complexes, confirming an intermediate oxidation state (Table 2).

Additionally, compound 16 was proposed to be mononuclear Pd(II)-hydroxide species in solution, despite X-ray crystallography only isolating a solid-state binuclear Pd(II) complex (1).⁴⁷ Figure 7 shows that the K-edge energy for the mononuclear compound 16 is higher than that for the

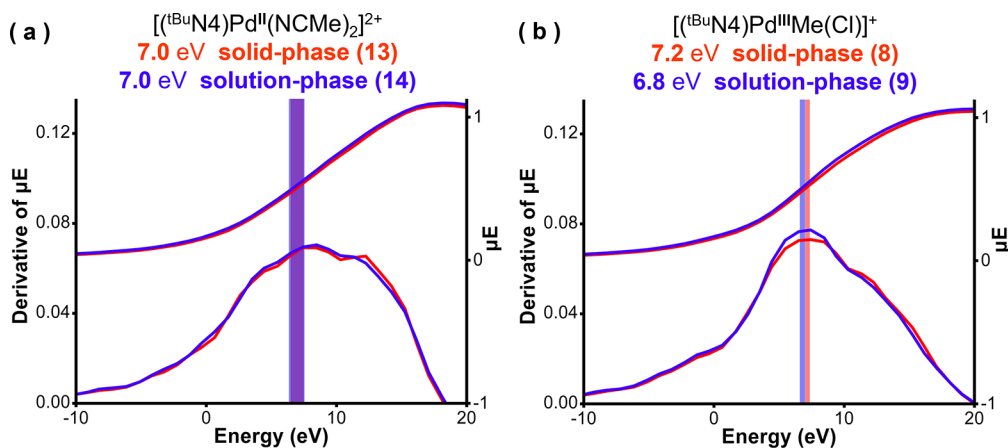


Figure 6. Comparison of solution phase samples 9 and 14 (blue) with their analogous solid phase samples 8 and 13 (red), respectively. The top lines show the XANES normalized energy curves corresponding to the rightmost y-axes, while the bottom lines show their derivatives corresponding to the leftmost y-axes. The difference in K-edge energies between phases is not statistically significant, as shown by the overlapping vertical lines that depict the fit errors.

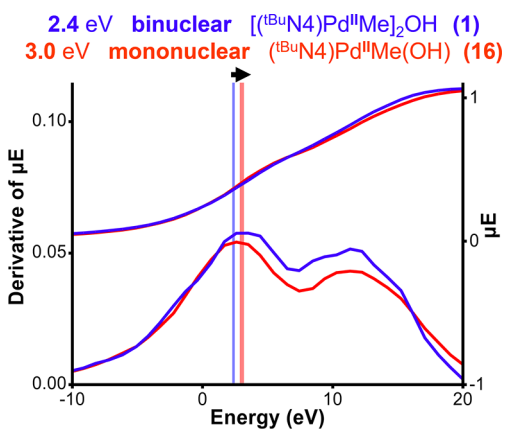


Figure 7. Comparison of the XANES K-edge energies of ${}^{\text{tBu}}\text{N}_4\text{Pd}^{\text{II}}\text{Me}(\text{OH})$ upon dimerization with the bridging hydroxide group. The top lines show the XANES normalized energy curves corresponding to the rightmost y-axes, while the bottom lines show their derivatives corresponding to the leftmost y-axes. The mononuclear compound 16 is higher in energy than the binuclear compound 1, supporting that there is less electron density on the binuclear Pd centers, as they are sharing one hydroxide group. Vertical lines indicate the K-edge energy where the width indicates the error on either side.

binuclear complex 1, consistent with reduced electron density on the two Pd centers due to them now sharing a single bridging hydroxide (Figure 1).

Peak Fitting Considerations. As shown in Figure 2 and Table S1, the highest intensity peak in the first derivative of the normalized XANES spectra was determined to be the K-edge energy. The exact value was extracted using a 3-Gaussian fit to isolate three distinct peaks, and then the peak that corresponded with the highest intensity point from the first derivative was chosen. In almost all cases with two major peaks, the leftmost peak was the most intense, consistent with the choice of referencing all data to the leftmost peak of the Pd foil (Figure 2). Only compound 24 had the highest energy 11.3 eV peak as the most intense peak, but peak fitting confirmed that the leftmost peak at 4.5 eV was the major contributor based on peak integration, as shown in the Supporting Information, Section II. In general, integrating peak values did have limitations as many of the 3-Gaussian fits would fit two broader peaks with higher errors than the primary sharp peak that corresponded with the maximum of the first derivative. For instance, compounds 1/7/12/15/17/26 have additional broad peaks with large errors that integrate to a value higher than that of the most intense peak we determined to be the K-edge. Conversely, compounds 21/22/23/25/26 all have one primary peak, and unlike all other

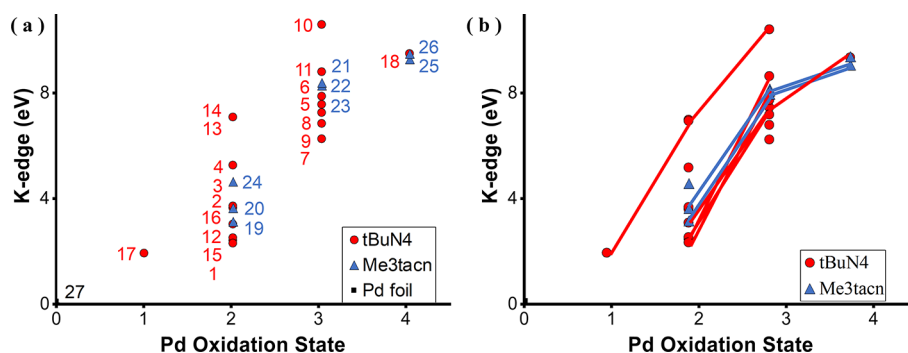


Figure 8. Correlations between oxidation states with K-edge energies, reported for the lower energy and often highest intensity peak, (a) across all compounds 1–26 (with $R^2 = 0.88$ for Me_3tacn and $R^2 = 0.70$ for ${}^{\text{tBu}}\text{N}_4$ for the linear fits), and (b) with connections drawn between analogous ligand systems across Pd(I)–Pd(IV) systems. Compounds supported by Me_3tacn are shown in blue, while those supported by ${}^{\text{tBu}}\text{N}_4$ are shown in red. Further analysis is shown in Supporting Information Section VI.

compounds, there is no trace of a higher energy peak. Further comparisons between these different methods of getting a K-edge energy are shown in Table S3 and Figure S14, which depict poor trends when using the highest energy peak, the energy gap between peaks, and the peak with the largest integration. Additionally, fitting extracted peak value from a 3-Gaussian fit gave a better trend than just using the highest intensity point of the first derivative (Figure 8).

CONCLUSIONS

Comparison of K-edge energies revealed that for similar ligand environments, a higher oxidation state has a higher K-edge energy: Pd(I) < Pd(II) < Pd(III) < Pd(IV). Using two different ligand backbones, Me₃tacn and ^tBu₄N⁺, we observed that K-edge energies increase along with the coordination number, going from 4- to 5- and 6-coordinate metal centers, while also providing insight into the degeneracy of the 5p orbitals. The Pd K-edge energies also increased when substituting strong σ -donating methyl groups with weaker field π -donating ligands such as chlorides, consistent with a qualitative ligand field analysis where π -donating ligands lead to an increase of the energy of the π -antibonding metal-based orbitals. Additionally, increasing the overall charge of the complex by replacing charged ligands (i.e., halides and methyl) with neutral ligands (i.e., acetonitrile) increased the K-edge energies. We were also able to distinguish between mononuclear and binuclear species, which is particularly useful for cases in which paramagnetic states are coupled. Overall, this study of a series of 25 palladium complexes in varying ligand environments provides important insights into the use of XAS to study *in situ* Pd systems to monitor ligand substitution, change in the coordination environment, and redox reactions.

ASSOCIATED CONTENT

Supporting Information

The Supporting Information is available free of charge at <https://pubs.acs.org/doi/10.1021/acs.inorgchem.3c03032>.

Additional figures including comparisons of XANES spectra, the synthesis and characterization of compounds, and CIF files (PDF)

Accession Codes

CCDC 2214382 contains the supplementary crystallographic data for this paper. These data can be obtained free of charge via www.ccdc.cam.ac.uk/data_request/cif, or by emailing data_request@ccdc.cam.ac.uk, or by contacting The Cambridge Crystallographic Data Centre, 12 Union Road, Cambridge CB2 1EZ, UK; fax: +44 1223 336033.

AUTHOR INFORMATION

Corresponding Author

Liviu M. Mirica – Department of Chemistry, University of Illinois at Urbana–Champaign, Urbana, Illinois 61801, United States; orcid.org/0000-0003-0584-9508; Email: mirica@illinois.edu

Authors

Luke P. Westawker – Department of Chemistry, University of Illinois at Urbana–Champaign, Urbana, Illinois 61801, United States

Julia K. Khusnutdinova – Coordination Chemistry and Catalysis Unit, Okinawa Institute of Science and Technology Graduate University, Okinawa 904-0495, Japan

Rachel F. Wallick – Department of Chemistry, University of Illinois at Urbana–Champaign, Urbana, Illinois 61801, United States; orcid.org/0000-0002-7548-4850

Complete contact information is available at:

<https://pubs.acs.org/10.1021/acs.inorgchem.3c03032>

Notes

The authors declare no competing financial interest.

ACKNOWLEDGMENTS

We thank the National Science Foundation (CHE-2102544 to L.M.M.) for financial support. L.P.W. acknowledges support from the National Science Foundation Graduate Research Fellowship Program. We also thank Drs. Jeffrey T. Miller and Ryan C. Nelson (Argonne National Lab) for assistance with obtaining the XAS data. X-ray absorption measurements were performed at the insertion-device beamline of the Materials Research Collaborative Access Team (MRCAT) at the Advanced Photon Source (APS) located within the Argonne National Laboratory. MRCAT operations are supported by the Department of Energy and the MRCAT member institutions. This research used resources of the Advanced Photon Source, a U.S. Department of Energy (DOE) Office of Science User Facility operated for the DOE Office of Science by Argonne National Laboratory under contract no. DE-AC02-06CH11357 operated by UChicago Argonne, LLC.

REFERENCES

- (1) Lee, P. A.; Citrin, P. H.; Eisenberger, P.; Kincaid, B. M. Extended X-Ray Absorption Fine-Structure - Its Strengths and Limitations as a Structural Tool. *Rev. Modern Physics* **1981**, *53* (4), 769–806.
- (2) Bertagnolli, H.; Ertel, T. S. X-Ray-Absorption Spectroscopy of Amorphous Solids, Liquids, and Catalytic and Biochemical Systems - Capabilities and Limitations. *Angew. Chem., Int. Ed.* **1994**, *33* (1), 45–66.
- (3) Singh, J.; Lamberti, C.; van Bokhoven, J. A. Advanced X-ray absorption and emission spectroscopy: *in situ* catalytic studies. *Chem. Soc. Rev.* **2010**, *39* (12), 4754–4766.
- (4) Bare, S. R.; Kelly, S. D.; Ravel, B.; Greenlay, N.; King, L.; Mickelson, G. E. Characterizing industrial catalysts using *in situ* XAFS under identical conditions. *Phys. Chem. Chem. Phys.* **2010**, *12* (27), 7702–7711.
- (5) Chisholm-Brause, C. J.; O'Day, P. A.; Brown, G. E.; Parks, G. A. Evidence for Multinuclear Metal-Ion Complexes at Solid Water Interfaces from X-Ray Absorption-Spectroscopy. *Nature* **1990**, *348* (6301), 528–531.
- (6) Gambardella, A. A.; Cotte, M.; de Nolf, W.; Schnetz, K.; Erdmann, R.; van Elsas, R.; Gonzalez, V.; Wallert, A.; Iedema, P. D.; Eveno, M.; Keune, K. Sulfur K-edge micro- and full-field XANES identify marker for preparation method of ultramarine pigment from lapis lazuli in historical paints. *Sci. Adv.* **2020**, *6* (18), No. eaay8782, DOI: [10.1126/sciadv.aay8782](https://doi.org/10.1126/sciadv.aay8782).
- (7) Timoshenko, J.; Cuenya, B. R. *In Situ/Operando* Electrocatalyst Characterization by X-ray Absorption Spectroscopy. *Chem. Rev.* **2021**, *121* (2), 882–961.
- (8) Hummer, A. A.; Rompel, A. X-Ray Absorption Spectroscopy: A Tool to Investigate the Local Structure of Metal-Based Anticancer Compounds *In Vivo*. *Adv. Protein Chem. Struct. Biol.* **2013**, *93*, 257–305.
- (9) Fulton, J. L.; Linehan, J. C.; Autrey, T.; Balasubramanian, M.; Chen, Y.; Szymczak, N. K. When is a nanoparticle a cluster? An

- operando EXAFS study of amine borane dehydrocoupling by Rh4–6 clusters. *J. Am. Chem. Soc.* **2007**, *129* (39), 11936–11949.
- (10) van der Veen, R. M.; Kas, J. J.; Milne, C. J.; Pham, V. T.; El Nahhas, A.; Lima, F. A.; Vithanage, D. A.; Rehr, J. J.; Abela, R.; Chergui, M. L-edge XANES analysis of photoexcited metal complexes in solution. *Phys. Chem. Chem. Phys.* **2010**, *12* (21), 5551–5561.
- (11) Bauer, M.; Gastl, C. X-Ray absorption in homogeneous catalysis research: the iron-catalyzed Michael addition reaction by XAS, RIXS and multi-dimensional spectroscopy. *Phys. Chem. Chem. Phys.* **2010**, *12* (21), 5575–5584.
- (12) Battocchio, C.; D'Acapito, F.; Fratoddi, I.; La Groia, A.; Polzonetti, G.; Roviello, G.; Russo, M. V. Platinum (II) dialkynyl bridged binuclear complex and related multinuclear oligomer: Comparison of EXAFS and X-ray crystal structure studies. *Chem. Phys.* **2006**, *328* (1–3), 269–274.
- (13) Berry, J. F.; Bill, E.; Bothe, E.; George, S. D.; Mienert, B.; Neese, F.; Wieghardt, K. An octahedral coordination complex of iron(VI). *Science* **2006**, *312* (5782), 1937–1941.
- (14) Rohde, J. U.; Betley, T. A.; Jackson, T. A.; Saouma, C. T.; Peters, J. C.; Que, L. XAS characterization of a Nitridoiron(IV) complex with a very short Fe–N bond. *Inorg. Chem.* **2007**, *46* (14), 5720–5726.
- (15) Chatterjee, R.; Weninger, C.; Loukianov, A.; Gul, S.; Fuller, F. D.; Cheah, M. H.; Fransson, T.; Pham, C. C.; Nelson, S.; Song, S.; Britz, A.; Messinger, J.; Bergmann, U.; Alonso-Mori, R.; Yachandra, V. K.; Kern, J.; Yano, J. XANES and EXAFS of dilute solutions of transition metals at XFELs. *J. Synchrotron Radiat.* **2019**, *26*, 1716–1724.
- (16) Baker, M. L.; Mara, M. W.; Yan, J. J.; Hodgson, K. O.; Hedman, B.; Solomon, E. I. K- and L-edge X-ray absorption spectroscopy (XAS) and resonant inelastic X-ray scattering (RIXS) determination of differential orbital covalency (DOC) of transition metal sites. *Coord. Chem. Rev.* **2017**, *345*, 182–208.
- (17) Nelson, R. C.; Miller, J. T. An introduction to X-ray absorption spectroscopy and its in situ application to organometallic compounds and homogeneous catalysts. *Catal. Sci. Technol.* **2012**, *2* (3), 461–470.
- (18) Patel, P.; Lu, Z.; Jafari, M. G.; Hernandez-Prieto, C.; Zatsopin, P.; Mendiola, D. J.; Kaphan, D. M.; Delferro, M.; Kropf, J.; Liu, C. Integrated Experimental and Computational K-Edge X-ray Absorption Near-Edge Structure Analysis of Vanadium Catalysts. *J. Phys. Chem. C* **2022**, *126* (29), 11949–11962.
- (19) Zhu, J.; Zeng, Z. H.; Li, W. X. K-Edge XANES Investigation of Fe-Based Oxides by Density Functional Theory Calculations. *J. Phys. Chem. C* **2021**, *125* (47), 26229–26239.
- (20) Nomura, K.; Izawa, I.; Yi, J.; Nakatani, N.; Aoki, H.; Harakawa, H.; Ina, T.; Mitsudome, T.; Tomotsu, N.; Yamazoe, S. Solution XAS Analysis for Exploring Active Species in Syndiospecific Styrene Polymerization and 1-Hexene Polymerization Using Half-Titanocene-MAO Catalysts: Significant Changes in the Oxidation State in the Presence of Styrene. *Organometallics* **2019**, *38* (22), 4497–4507.
- (21) Nomura, K.; Mitsudome, T.; Igarashi, A.; Nagai, G.; Tsutsumi, K.; Ina, T.; Omiya, T.; Takaya, H.; Yamazoe, S. Synthesis of (Adamantylimido)vanadium(V) Dimethyl Complex Containing (2-Anilidomethyl)pyridine Ligand and Selected Reactions: Exploring the Oxidation State of the Catalytically Active Species in Ethylene Dimerization. *Organometallics* **2017**, *36* (3), 530–542.
- (22) Boysen, R. B.; Szilagyi, R. K. Development of palladium L-edge X-ray absorption spectroscopy and its application for chloropalladium complexes. *Inorg. Chim. Acta* **2008**, *361* (4), 1047–1058.
- (23) Barton, R. L.; Gardenghi, D. J.; Stolte, W. C.; Szilagyi, R. K. Multiedge X-ray Absorption Spectroscopy Part II: XANES Analysis of Bridging and Terminal Chlorides in Hexachlorodipalladate(II) Complex. *J. Phys. Chem. A* **2015**, *119* (22), 5579–5586.
- (24) Lyons, T. W.; Sanford, M. S. Palladium-Catalyzed Ligand-Directed C–H Functionalization Reactions. *Chem. Rev.* **2010**, *110* (2), 1147–1169.
- (25) Muniz, K. High-Oxidation-State Palladium Catalysis: New Reactivity for Organic Synthesis. *Angew. Chem., Int. Ed.* **2009**, *48* (50), 9412–9423.
- (26) Canty, A. J. Organopalladium and platinum chemistry in oxidising milieu as models for organic synthesis involving the higher oxidation states of palladium. *Dalton Trans.* **2009**, *47*, 10409–10417.
- (27) Chen, X.; Engle, K. M.; Wang, D.-H.; Yu, J.-Q. Palladium(II)-Catalyzed C–H Activation/C–C Cross-Coupling Reactions: Versatility and Practicality. *Angew. Chem., Int. Ed.* **2009**, *48* (28), 5094–5115.
- (28) Sehnal, P.; Taylor, R. J. K.; Fairlamb, I. J. S. Emergence of Palladium(IV) Chemistry in Synthesis and Catalysis. *Chem. Rev.* **2010**, *110* (2), 824–889.
- (29) Desai, L. V.; Hull, K. L.; Sanford, M. S. Palladium-catalyzed oxygenation of unactivated sp(3) C–H bonds. *J. Am. Chem. Soc.* **2004**, *126* (31), 9542–9543.
- (30) Xu, L. M.; Li, B. J.; Yang, Z.; Shi, Z. J. Organopalladium(IV) chemistry. *Chem. Soc. Rev.* **2010**, *39* (2), 712–733.
- (31) Powers, D. C.; Ritter, T. Palladium(III) in Synthesis and Catalysis. *Top. Organomet. Chem.* **2011**, *35*, 129–156.
- (32) Mirica, L. M.; Khusnutdinova, J. R. Structure and electronic properties of Pd(III) complexes. *Coord. Chem. Rev.* **2013**, *257* (2), 299–314.
- (33) Henry, P. M. *Palladium Catalyzed Oxidation of Hydrocarbons*. D. Reidel Publishing Company: Boston, 1980; p 435 DOI: 10.1007/978-94-009-9446-1.
- (34) Negishi, E.-I. *Handbook of Organopalladium Chemistry for Organic Synthesis*. John Wiley & Sons, Inc.: Hoboken, NJ, 2002; p 3424 DOI: 10.1002/0471212466.
- (35) Hartwig, J. F. *Organotransition Metal Chemistry: From Bonding to Catalysis*. University Science Books: Sausalito, Calif., 2010; p 1127.
- (36) Khusnutdinova, J. R.; Rath, N. P.; Mirica, L. M. The Conformational Flexibility of the Tetradentate Ligand tBuN4 is Essential for the Stabilization of (tBuN4)Pd(III) Complexes. *Inorg. Chem.* **2014**, *53* (24), 13112–13129.
- (37) Canty, A. J. Development of organopalladium(IV) chemistry: fundamental aspects and systems for studies of mechanism in organometallic chemistry and catalysis. *Acc. Chem. Res.* **1992**, *25* (2), 83–90.
- (38) Racowski, J. M.; Sanford, M. S. Carbon–Heteroatom Bond-Forming Reductive Elimination from Palladium(IV) Complexes. *Top. Organomet. Chem.* **2011**, *35*, 61–84.
- (39) Daugulis, O.; Do, H.-Q.; Shabashov, D. Palladium- and Copper-Catalyzed Arylation of Carbon-Hydrogen Bonds. *Acc. Chem. Res.* **2009**, *42* (8), 1074–1086.
- (40) Engle, K. M.; Mei, T.-S.; Wasa, M.; Yu, J.-Q. Weak Coordination as a Powerful Means for Developing Broadly Useful C–H Functionalization Reactions. *Acc. Chem. Res.* **2012**, *45* (6), 788–802.
- (41) Kalyani, D.; Dick, A. R.; Anani, W. Q.; Sanford, M. S. Scope and selectivity in palladium-catalyzed directed C–H bond halogenation reactions. *Tetrahedron* **2006**, *62* (49), 11483–11498.
- (42) Rosen, B. R.; Simke, L. R.; Thuy-Boun, P. S.; Dixon, D. D.; Yu, J.-Q.; Baran, P. S. C–H Functionalization Logic Enables Synthesis of (+)-Hongoquercin A and Related Compounds. *Angew. Chem., Int. Ed.* **2013**, *52*, 7317–7320.
- (43) Yamaguchi, J.; Yamaguchi, A. D.; Itami, K. C–H Bond Functionalization: Emerging Synthetic Tools for Natural Products and Pharmaceuticals. *Angew. Chem., Int. Ed.* **2012**, *51* (36), 8960–9009.
- (44) Gray, H. B.; Ballhausen, C. J. A Molecular Orbital Theory for Square Planar Metal Complexes. *J. Am. Chem. Soc.* **1963**, *85* (3), 260–265.
- (45) Khusnutdinova, J. R.; Rath, N. P.; Mirica, L. M. Stable Mononuclear Organometallic Pd(III) Complexes and Their C–C Bond Formation Reactivity. *J. Am. Chem. Soc.* **2010**, *132* (21), 7303–7305.
- (46) Khusnutdinova, J. R.; Rath, N. P.; Mirica, L. M. Dinuclear Palladium(III) Complexes with a Single Unsupported Bridging Halide Ligand: Reversible Formation from Mononuclear Palladium-

- (II) or Palladium(IV) Precursors. *Angew. Chem., Int. Ed.* **2011**, *50* (24), 5532–5536.
- (47) Khusnutdinova, J. R.; Rath, N. P.; Mirica, L. M. The Aerobic Oxidation of a Pd(II) Dimethyl Complex Leads to Selective Ethane Elimination from a Pd(III) Intermediate. *J. Am. Chem. Soc.* **2012**, *134*, 2414–2422.
- (48) Khusnutdinova, J. R.; Mirica, L. M., Chapter 5: Organometallic Pd^{III} Complexes in C-C and C-Heteroatom Bond Formation Reactions. In *C-H and C-X Bond Functionalization: Transition Metal Mediation*, Ribas, X., Ed. Royal Society of Chemistry: 2013; pp 122–158.
- (49) Luo, J.; Khusnutdinova, J. R.; Rath, N. P.; Mirica, L. M. Unsupported d⁸-d⁸ interactions in cationic Pd^{II} and Pt^{II} complexes: Evidence for a significant metal-metal bonding character. *Chem. Commun.* **2012**, *48* (10), 1532–1534.
- (50) Tang, F. Z.; Qu, F. R.; Khusnutdinova, J. R.; Rath, N. P.; Mirica, L. M. Structural and reactivity comparison of analogous organometallic Pd(III) and Pd(IV) complexes. *Dalton Trans.* **2012**, *41* (46), 14046–14050.
- (51) Tang, F. Z.; Zhang, Y.; Rath, N. P.; Mirica, L. M. Detection of Pd(III) and Pd(IV) Intermediates during the Aerobic Oxidative C-C Bond Formation from a Pd(II) Dimethyl Complex. *Organometallics* **2012**, *31* (18), 6690–6696.
- (52) Luo, J.; Rath, N. P.; Mirica, L. M. Oxidative Reactivity of (N2S2)PdRX Complexes (R = Me, Cl; X = Me, Cl, Br): Involvement of Palladium(III) and Palladium(IV) Intermediates. *Organometallics* **2013**, *31* (11), 3343–3353.
- (53) Duan, H.; Li, M. H.; Zhang, G. H.; Gallagher, J. R.; Huang, Z. L.; Sun, Y.; Luo, Z.; Chen, H. Z.; Miller, J. T.; Zou, R. Q.; Lei, A. W.; Zhao, Y. L. Single-Site Palladium(II) Catalyst for Oxidative Heck Reaction: Catalytic Performance and Kinetic Investigations. *ACS Catal.* **2015**, *5* (6), 3752–3759.
- (54) Yuan, N.; Majeed, M. H.; Bajnoczi, E. G.; Persson, A. R.; Wallenberg, L. R.; Inge, A. K.; Heidenreich, N.; Stock, N.; Zou, X. D.; Wendt, O. F.; Persson, I. In situ XAS study of the local structure and oxidation state evolution of palladium in a reduced graphene oxide supported Pd(II) carbene complex during an undirected C-H acetoxylation reaction. *Catal. Sci. Technol.* **2019**, *9* (8), 2025–2031.
- (55) Tomson, N. C.; Labios, L. A.; Weyhermuller, T.; Figueroa, J. S.; Wieghardt, K. Redox Noninnocence of Nitrosoarene Ligands in Transition Metal Complexes. *Inorg. Chem.* **2011**, *50* (12), 5763–5776.
- (56) Tromp, M.; van Bokhoven, J. A.; van Strijdonck, G. P. F.; van Leeuwen, P. W. N. M.; Koningsberger, D. C.; Ramaker, D. E. Probing the molecular orbitals and charge redistribution in organometallic (PP)Pd(XX) complexes. A PdK-Edge XANES study. *J. Am. Chem. Soc.* **2005**, *127* (2), 777–789.
- (57) Luo, J.; Tran, G. N.; Rath, N. P.; Mirica, L. M. Detection and Characterization of Mononuclear Pd(I) Complexes Supported by N2S2 and N4 Tetradentate Ligands. *Inorg. Chem.* **2020**, *59*, 15659–15669.
- (58) Ittel, S. D.; Johnson, L. K.; Brookhart, M. Late-metal catalysts for ethylene homo- and copolymerization. *Chem. Rev.* **2000**, *100* (4), 1169–1203.
- (59) Meneghetti, S. P.; Lutz, P. J.; Kress, J. Neutral and Cationic Palladium(II) Complexes of a Diazapyridinophane. Structure, Fluxionality, and Reactivity toward Ethylene. *Organometallics* **2001**, *20* (24), 5050–5055.
- (60) Tang, F. Z.; Park, S. V.; Rath, N. P.; Mirica, L. M. Electronic versus steric effects of pyridinophane ligands on Pd(III) complexes. *Dalton Trans.* **2018**, *47* (4), 1151–1158.
- (61) Sinha, S.; Mirica, L. M. Electrocatalytic O₂ Reduction by an Organometallic Pd(III) Complex via a Binuclear Pd(III) Intermediate. *ACS Catal.* **2021**, *11* (9), 5202–5211.
- (62) Luo, J.; Tran, G. N.; Rath, N. P.; Mirica, L. M. Detection and Characterization of Mononuclear Pd(I) Complexes Supported by N2S2 and N4 Tetradentate Ligands. *Inorg. Chem.* **2020**, *59* (21), 15659–15669.
- (63) Khusnutdinova, J. R.; Rath, N. P.; Mirica, L. M. Dinuclear Palladium(III) Complexes with a Single Unsupported Bridging Halide Ligand: Reversible Formation from Mononuclear Palladium(II) or Palladium(IV) Precursors. *Angew. Chem., Int. Ed.* **2011**, *50* (24), 5532–5536.
- (64) Mirica, L. M.; Khusnutdinova, J. R. Structure and Electronic Properties of Pd(III) Complexes. *Coord. Chem. Rev.* **2013**, *257*, 299–314.
- (65) Blake, A. J.; Holder, A. J.; Roberts, Y. V.; Schröder, M. Agostic Pd···H+···NHR₂ and apical Pd···NHR₂ interactions: the synthesis and structures of [PdIICl₂(H[9]aneN₃)]⁺, the PdII-PdII dimer [(H[9]aneN₃)Cl₂Pd-PdCl₂(H[9]aneN₃)]²⁺, and [Pd(Me₃[9]aneN₃)(NCMe)₂]²⁺. *J. Chem. Soc., Chem. Commun.* **1993**, *3*, 260–262.
- (66) Kropf, A. J.; Katsoudas, J.; Chattopadhyay, S.; Shibata, T.; Lang, E. A.; Zyryanov, V. N.; Ravel, B.; McIvor, K.; Kemner, K. M.; Scheckel, K. G.; Bare, S. R.; Terry, J.; Kelly, S. D.; Bunker, B. A.; Segre, C. U. The New MRCAT (Sector 10) Bending Magnet Beamline at the Advanced Photon Source. *AIP Conf. Proc.* **2010**, *1234*, 299–302.
- (67) Segre, C. U.; Leyarovska, N. E.; Chapman, L. D.; Lavender, W. M.; Plag, P. W.; King, A. S.; Kropf, A. J.; Bunker, B. A.; Kemner, K. M.; Dutta, P.; Duran, R. S.; Kaduk, J. The MRCAT insertion device beamline at the Advanced Photon Source. *AIP Conf. Proc.* **2000**, *521*, 419–422.
- (68) Ravel, B.; Newville, M. ATHENA, ARTEMIS, HEPHAESTUS: data analysis for X-ray absorption spectroscopy using. *J. Synchrotron Radiat.* **2005**, *12*, 537–541.
- (69) Bearden, J. A.; Burr, A. F. Reevaluation of X-Ray Atomic Energy Levels. *Rev. Modern Physics* **1967**, *39* (1), 125–142.